X-ray Structures of *Torpedo californica* Acetylcholinesterase Complexed with (+)-Huperzine A and (−)-Huperzine B: Structural Evidence for an Active Site Rearrangement[†,‡]

H. Dvir,[§,||] H. L. Jiang,[§,⊥] D. M. Wong,[§,||] M. Harel,[§] M. Chetrit,[§] X. C. He,[⊥] G. Y. Jin,[⊥] G. L. Yu,[⊥] X. C. Tang,[⊥] I. Silman,[||] D. L. Bai,*[,⊥] and J. L. Sussman*[,§]

Departments of Structural Biology and Neurobiology, Weizmann Institute of Science, Rehovot 76100, Israel, and State Key Laboratory of Drug Research, Shanghai Institute of Materia Medica, Shanghai Institutes for Biological Sciences, Chinese Academy of Sciences, Shanghai 200031, Peoples Republic of China

Received February 20, 2002; Revised Manuscript Received June 26, 2002

ABSTRACT: Kinetic and structural data are presented on the interaction with *Torpedo californica* acetylcholinesterase (*Tc*AChE) of (+)-huperzine A, a synthetic enantiomer of the anti-Alzheimer drug, (−)-huperzine A, and of its natural homologue (−)-huperzine B. (+)-Huperzine A and (−)-huperzine B bind to the enzyme with dissociation constants of 4.30 and 0.33 μM, respectively, compared to 0.18 μM for (−)-huperzine A. The X-ray structures of the complexes of (+)-huperzine A and (−)-huperzine B with *Tc*AChE were determined to 2.1 and 2.35 Å resolution, respectively, and compared to the previously determined structure of the (−)-huperzine A complex. All three interact with the "anionic" subsite of the active site, primarily through $\pi-\pi$ stacking and through van der Waals or C−H$\cdots\pi$ interactions with Trp84 and Phe330. Since their α-pyridone moieties are responsible for their key interactions with the active site via hydrogen bonding, and possibly via C−H$\cdots\pi$ interactions, all three maintain similar positions and orientations with respect to it. The carbonyl oxygens of all three appear to repel the carbonyl oxygen of Gly117, thus causing the peptide bond between Gly117 and Gly118 to undergo a peptide flip. As a consequence, the position of the main chain nitrogen of Gly118 in the "oxyanion" hole in the native enzyme becomes occupied by the carbonyl of Gly117. Furthermore, the flipped conformation is stabilized by hydrogen bonding of Gly117O to Gly119N and Ala201N, the other two functional elements of the three-pronged "oxyanion hole" characteristic of cholinesterases. All three inhibitors thus would be expected to abolish hydrolysis of all ester substrates, whether charged or neutral.

The most common form of dementia in adults, Alzheimer's disease (AD),[1] is characterized by developing cholinergic deficit as the disease progresses (*1*). Progressive deterioration of memory and learning is a characteristic manifestation of AD (*2*). The progression of the disease symptoms is associated with structural changes in cholinergic synapses in certain brain regions and consequent impairment of cholinergic neurotransmission (*3*). These factors result in a decrease in the amounts released of the neurotransmitter acetylcholine (ACh). The enzyme acetylcholinesterase (AChE; EC 3.1.1.7) functions in cholinergic synapses of the central and peripheral nervous systems, where its principal biological role is termination of impulse transmission by rapid hydrolysis of ACh (*4*). The "cholinergic hypothesis" suggested that inhibition of AChE might thus ameliorate the symptoms of the disease. This led to the development of cholinergic therapies for AD using AChE inhibitors as drugs (*5*−*7*). The inhibitors approved so far include synthetic compounds such as tacrine, marketed as Cognex (*8*), E2020, marketed as Aricept (*9*), and rivastigmine, marketed as Exelon (*10*). Among the natural inhibitors of AChE, galanthamine, under its trade name Reminyl (*11*), and (−)-huperzine A [(−)-HupA] (*12*) have been approved. Crystal structures of each of the above drugs in complex with *Torpedo californica*

[†] This work was supported by the U.S. Army Medical and Materiel Command under Contract DAMD17-97-2-7022, the EC Fifth Framework Program on the Quality of Life and Management of Living Resources, the Kimmelman Center for Biomolecular Structure and Assembly (Rehovot, Israel), and the Benoziyo Center for Neurosciences. I.S. is the Bernstein-Mason Professor of Neurochemistry. Also supported by the National Natural Science Foundation of China (Grants 29725203, 39770846, and 30070865), the "863" High-Tech Program of China (Grant 863-103-04-01), the State Key Program of Basic Research of China (Grants 2001AA235041 and 2001AA235051), and the Ministry of Science and Technology of Shanghai (Grant 98JjC14028).

[‡] Coordinates and structure factors for the structures of the complexes of *Tc*AChE with (−)-huperzine B and (+)-huperzine A have been deposited at the Protein Data Bank with the respective accession codes 1GPN and 1GPK.

* Corresponding authors. D.L.B.: tel, 86-21-64311833 ext 628; fax, 86-21-64370269; e-mail, dlbai@mail.shcnc.ac.cn. J.L.S.: tel, 972-8-9344531; fax, 972-8-9344159; e-mail, joel.sussman@weizmann.ac.il.

[§] Department of Structural Biology, Weizmann Institute of Science.

[||] Department of Neurobiology, Weizmann Institute of Science.

[⊥] Shanghai Institutes for Biological Sciences, Chinese Academy of Sciences.

[1] Abbreviations: AChE, acetylcholinesterase (EC 3.1.1.7); *Tc*, *Torpedo californica*; ACh, acetylcholine; Hup, huperzine; NMDA, *N*-methyl-D-aspartate; MES, 2-(*N*-morpholino)ethanesulfonic acid; DTNB, 5,5′-dithiobis(2-nitrobenzoic acid); PEG, poly(ethylene glycol); AD, Alzheimer's disease; PDB, Protein Data Bank; ESRF, European Synchrotron Radiation Facility; CNS, Crystallography & NMR System; SA, simulated annealing; IB, individual *B*-factors; H-bond, hydrogen bond; AU, asymmetric unit.

10.1021/bi020151+ CCC: $22.00
Published on Web 08/07/2002

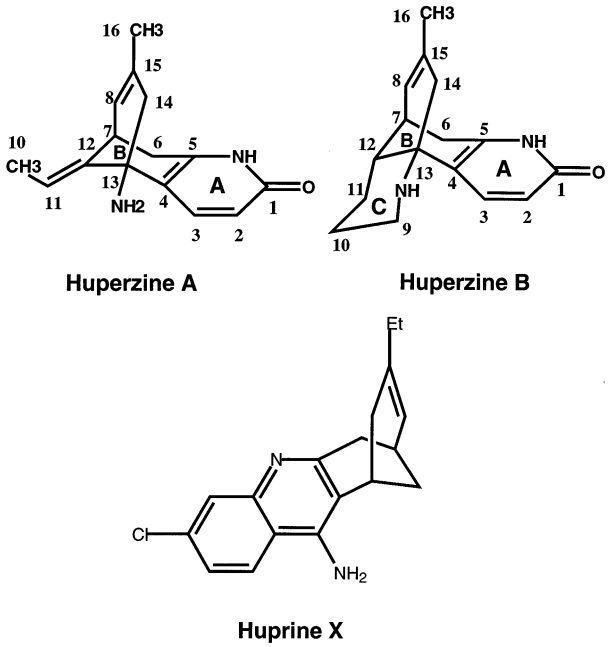

FIGURE 1: Chemical structures of AChE inhibitors referred to in the text.

AChE (*Tc*AChE) have been determined (*13*−*17*), and the principal governing interactions have been pinpointed.

(−)-HupA and (−)-huperzine B [(−)-HupB] (Figure 1) are two *Lycopodium* alkaloids isolated from the herb *Huperzia serrata*, which grows mainly in hilly regions in the provinces of southern China (*18*). This herb has been used in traditional Chinese medicine for centuries to treat contusion, strain, swelling, schizophrenia, and other ailments (*19*). Both compounds were found to inhibit AChE reversibly (*18*, *20*, *21*). Similarly to (−)-HupA, (−)-HupB was shown to be more specific for AChE, relative to butyrylcholinesterase, than galanthamine and tacrine (*22*). Thus, although (−)-HupB is less potent than tacrine in in vitro inhibition of *Tc*AChE, its selectivity for rat cortex AChE, relative to rat serum BuChE, is 120-fold higher, based on the IC_{50} values for the two enzymes. There have been extensive studies on the inhibition of AChE by (−)-HupA as a lead compound for the development of more effective drugs (*23*−*25*). Like (−)-HupA, (−)-HupB facilitated memory retention and retrieval in mice and improved impaired memory (*26*, *27*). At the same time it exhibited less peripheral side effects than galanthamine and physostigmine (*28*). These pharmacological features render (−)-HupB, like (−)-HupA, a promising candidate for AD therapy. Both (−)-HupA and (−)-HupB were shown to exert an antagonist effect on the *N*-methyl-D-aspartate (NMDA) receptor in rat cerebral cortex and thus could reduce neuronal cell death caused by glutamate (*29*, *30*). This dual action would be expected to increase the value of (−)-HupA and (−)-HupB as therapeutic agents for the treatment of AD and other neurodegenerative diseases.

More recently, the effects of (−)- and (+)-Hup A were compared both on the NMDA receptor (*31*) and in protection against β-amyloid (*25*−*35*) induced injury in PC12 and NG 108-15 neuroblastoma cell lines (*32*). The two enantiomers displayed similar potency toward the NMDA receptor and similar protection against β-amyloid toxicity. Thus the neuroprotective properties of HupA are not stereoselective. In contrast, the stereoselectivity of AChE for HupA is substantial, with the nonnatural enantiomorph, (+)-HupA, being almost 2 orders of magnitude less potent than (−)-HupA (*33*, *34*). On the basis of this observation and the structure of the complex with huprine X, (+)-HupA was speculated to bind to *Tc*AChE with its α-pyridone ring pointing in the opposite direction relative to that of (−)-HupA (*35*). This orientation is similar to that of the aromatic ring system of huprine X, which is a chemical hybrid of tacrine and HupA, which has a configuration that has more in common with that of (+)-HupA than with that of (−)-HupA. Yet, no crystallographic information has been reported for the complex of (+)-HupA with AChE, and the link between the stereoselectivity of AChE for HupA and the molecular interaction of the two stereoisomers with the active site has remained open. In the following, we describe the determination of the crystal structures of complexes of both (−)-HupB and (+)-HupA with *Tc*AChE and compare them to the previously determined structure of the complex with (−)-HupA (*16*). Since (−)-HupA displays a high degree of species specificity (*33*, *36*), it would have been too speculative to rationalize the interactions seen in the crystal structures with affinities determined for AChE from heterologous species. Thus, we also determined the steady-state

Table 1: X-ray Data Collection and Processing

parameters	(+)-HupA/*Tc*AChE	(−)-HupB/*Tc*AChE
space group	$P3_121$	$P3_121$
molecules (au)	1	1
cell axes (Å)/angles (deg)	111.4, 111.4, 137.1/ 90, 90, 120	111.7, 111.7, 137.1/ 90, 90, 120
X-ray source, beamline, wavelength (Å)	ESRF, ID14-2, 0.93260	ESRF, ID14-2, 0.93260
temperature (K)	100	100
resolution range (Å)	20−2.1	20−2.35
no. of measd reflections	677200	159761
no. of unique reflections	67270	50834
no. of reflections used	57502	41627
completeness, all data (highest shell)[a] (%)	98.8 (99.9)	98.3 (99.7)
R_{sym}, all data (highest shell) (%)	4.4 (41.6)	5.8 (22.5)
I/σ, all data (highest shell) (%)	15.2 (2.0)	14.9 (3.6)

[a] Ten is the number of resolution shells.

Table 2: Refinement Results

	*Tc*AChE/(−)-HupB	*Tc*AChE/(+)-HupA
resolution range (Å)	20−2.35	20−2.1
no. of protein atoms	4197	4235
no. of water molecules	289	529
no. of heterogen atoms (including inhibitor and carbohydrates)	47	74
R_{work} (%)	18.6	18.9
R_{free} (%)	21.6	21.4
RMSD, bond length (Å)	0.012	0.006
RMSD, bond angle (deg)	1.529	1.32
agreement with Ramachandran plot	90.2% in the most favorable region; two residues in the generously allowed region	89.8% in the most favorable region; three residues in the generously allowed region

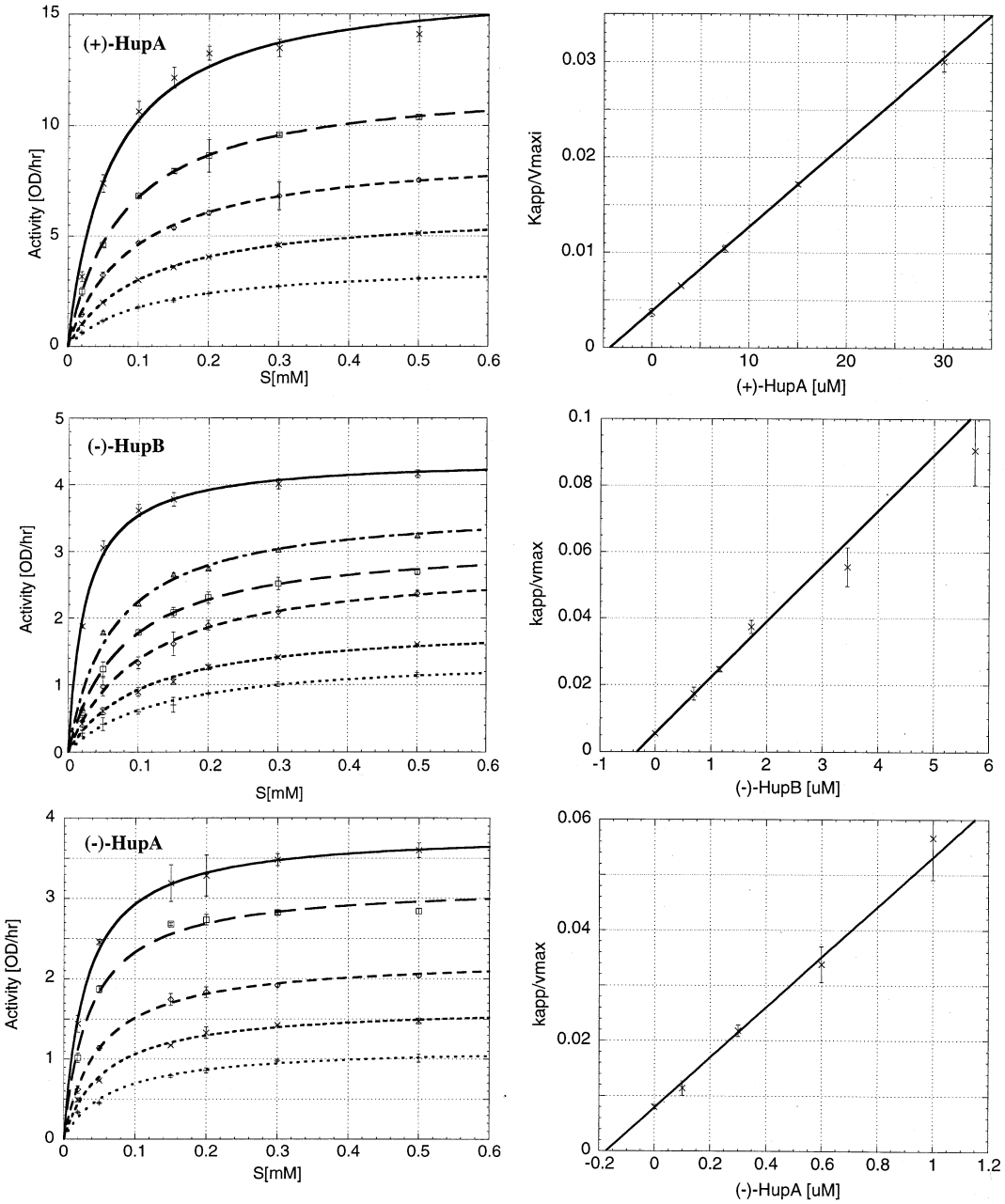

FIGURE 2: Steady-state inhibition of *Tc*AChE by (+)-HupA, (−)-HupA, and (−)-HupB. The left-hand side of the figure shows the fit of measured enzymatic activity as a function of substrate concentration to the Michaelis−Menten equation for several inhibitor concentrations in the vicinity of the corresponding IC_{50} values. The fit was performed in KaleidaGraph and allowed for a constant error of 0.1%. From each curve a value for K_{app}/V_{maxi} was calculated. Plots of these values as a function of the corresponding inhibitor concentration are given on the right. These values were linearly fit to the expression of K_{app}/V_{maxi}, as derived for a linear mixed-type inhibition (see Materials and Methods), using the reciprocals of their variances as weights. The Michaelis−Menten curves show a significant decrease in V_{max} values and a corresponding increase in K_m values as a function of inhibitor concentration (values not shown). Moreover, plots of K_{app}/V_{maxi}, as a function of the corresponding inhibitor concentration, are practically linear.

binding constants of (−)-HupA, (+)-HupA, and (−)-HupB for *Tc*AChE.

MATERIALS AND METHODS

Inhibitors. (−)-HupA and (−)-HupB were isolated from *H. serrata*, and the purities of both are >99.0%. (+)-HupA was prepared from (−)-methyl 9,10-dihydro-2-methoxy-7-methyl-11-oxo-5,9-methanocycloocta[*b*]pyridine-5(6H)-carboxylate, which was synthesized by the enantioselective palladium-catalyzed bicycloannulation of methyl 5,6,7,8-tetrahydro-2-methoxy-6-oxoquinoline-5-carboxylate with 2-methylene-1,3-propanediol diacetate, using a chiral ligand, ferrocenyl bisphosphine, (*S*)-*N*-cyclopentyl-*N*-(5-hydroxypentyl)-1-[(*R*)-1′,2-bis(diphenylphosphino)ferrocenyl]eth-

Table 3: Inhibition Constants of Inhibitors of *Tc*AChE

inhibitor	$K_i \pm$ SD (μM)
inhibition constants	
(−)-HupA	0.175 ± 0.017
(+)-HupA	4.300 ± 0.208
(−)-HupB	0.334 ± 0.029
ratios for above dissociation constants	
(+)-HupA/(−)-HupA	∼25
(+)-HupA/(−)-HupB	∼13
(−)-HupB/(−)-HupA	∼1.9

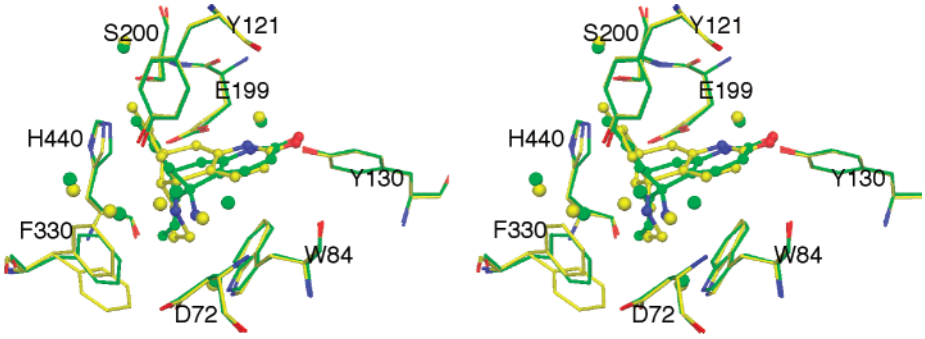

FIGURE 3: Stereoview of a superposition of complexed structures of *Tc*AChE/(−)-HupA (gray) and *Tc*AChE/(−)-HupB (yellow). Enzyme residues in the vicinity of the ligands are shown as stick models, while the ligands appear as balls and sticks. Oxygen atoms are colored red and nitrogens are colored blue. (−)-HupB and (−)-HupA are seen to occupy a very similar space at the bottom of the active site gorge of *Tc*AChE. Note the high similarity in the conformations of the amino acid residues around the ligands for the two structures, except that of Phe330, which is seen in two alternate conformations in the *Tc*AChE/(−)-HupB complex. The water network around (−)-HupB appears to be very similar to that seen around (−)-HupA.

ylamine. The >99.0% enantiomeric excess of (+)-HupA was determined by HPLC on a chiral column (Daicel AD, with hexane:2-propanol = 3:1 as eluent) (*37*).

Purification and Crystallization of TcAChE. The membrane-bound dimeric form of *Tc*AChE was solubilized and purified as described (*16*, *38*). A stock solution of the enzyme at 10−11 mg/mL in 1 mM 2-(*N*-morpholino)ethanesulfonic acid (MES), pH 6.5, 100 mM NaCl, and 0.02% NaN_3 was used for crystallization. Trigonal crystals were obtained as reported (*16*) and soaked in mother liquor containing saturating concentrations of either (+)-HupA or (−)-HupB for 3−10 days before X-ray data collection.

Steady-State Inhibition of AChE. After 25 min preincubation of the enzyme with the appropriate inhibitor, the reaction was initiated by addition of the substrate acetylthiocholine (Sigma, St. Louis, MO), and rates were obtained from initial velocities. Activity was followed by the spectrophotometric procedure of Ellman et al. (*39*) with 0.3 mM 5,5′-dithiobis(2-nitrobenzoic acid) (DTNB; Ellman's reagent; Sigma, St. Louis, MO). Reaction took place in a total volume of 350 μL consisting of 270 μL of phosphate buffer (10 mM Na_2HPO_4/NaH_2PO_4, pH 7.0, containing 50 mM NaCl and 0.01 mg/mL BSA), 35 μL of inhibitor solution in the same phosphate buffer, and 35 μL of substrate dissolved in water. Inhibitor concentrations were determined from their absorbance at λ_{max} using the following molar extinction coefficients: (±)-HupA, ϵ = 7762.47 M^{-1} cm^{-1} at 312 nm; (−)-HupB, ϵ = 7079.45 M^{-1} cm^{-1} at 313 nm (*18*). Activity was monitored on a TECAN Spectra Fluor Plus (Durham, NC) microplate reader at room temperature (≈25 °C). For both (−)-HupB and (−)-HupA, ca. 40 pM *Tc*AChE was used, yielding a reaction rate of ca. 0.06 ΔA/min, using 0.5 mM substrate in the absence of inhibitor. For (+)-HupA, an enzyme concentration was utilized that yielded ca. 0.23 ΔA/min under the same conditions. To preclude substrate inhibition, substrate concentrations were <0.5 mM. Treatment of the steady-state inhibition data for all of the inhibitors was as reported previously (*35*).

X-ray Data Collection. Data were collected at the ESRF (Grenoble, France) using beamline ID14-2 and a Bruker Smart 1500 based detector (BRUKER AXS, Madison, WI). Before mounting, crystals were dipped in oil (Paratone, EXXON) for cryoprotection (*40*, *41*). The crystal was then immediately fished out using a nylon cryoloop and flash-cooled to 100 K in an Oxford Cryosystems cooling apparatus (Oxford Cryosystems, Oxford, U.K.).

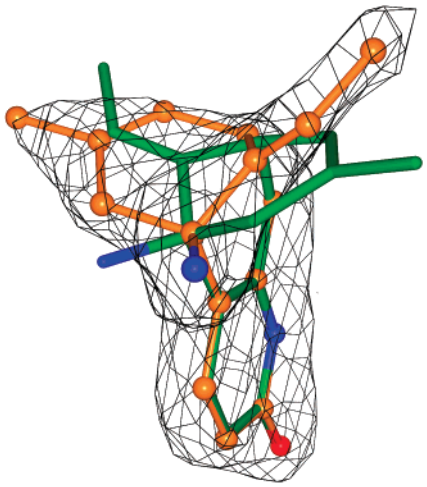

FIGURE 4: Modeling of (+)-HupA and (−)-HupA into the difference electron density map calculated for the *Tc*AChE/(+)-HupA. A $3F_o - 2F_c$ difference map was calculated on the basis of the coordinates of the native enzyme after one cycle of refinement against the data obtained for the *Tc*AChE/(+)-HupA complex; it does not suffer, therefore, from any model bias toward either of the two inhibitors. Although the α-pyridone moieties of both ligands fit the map equally well, their three-carbon bridges point in opposite directions. Thus, only the (+) enantiomer (orange ball-and-stick model) can be modeled correctly, with its primary amine, bridge methyl, and ethylidene methyl groups conforming very well to the electron density map, whereas the corresponding moieties of the (−) enantiomer (green stick model) clearly fit poorly.

Data collection was optimized by the program STRATEGY (*42*). Data processing was performed with DENZO and SCALEPACK (*43*). Data were truncated with the CCP4 program TRUNCATE (*44*), and a list of 5% randomly generated test reflections was used from a master list for the trigonal crystal form of *Tc*AChE. Reflections were output with MTZ2VARIOUS (*44*) to a format suitable for the CNS program (*45*). Table 1 summarizes pertinent information concerning X-ray data collection and processing.

Structure Determination and Refinement. The structures of both the *Tc*AChE/(+)-HupA and *Tc*AChE/(−)-HupB complexes were solved using the difference Fourier technique, exploiting the 1.8 Å native structure of *Tc*AChE (PDB ID code 1EA5) of the same space group, $P3_121$, and similar unit cell dimensions. Native structure coordinates were used

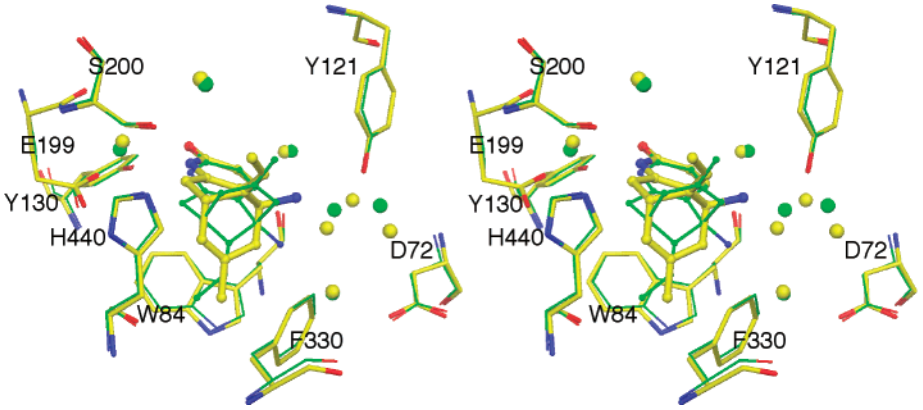

FIGURE 5: Stereoview of a superposition of two *Tc*AChE structures complexed with (−)-HupA (green) and (+)-HupA (yellow). Protein residues are shown as stick models with oxygen atoms colored red and nitrogens colored blue. The inhibitors are drawn as ball-and-stick models. All of the amino acid residues around the ligands are in very similar conformations. The ligands appear to occupy a similar binding site; however, because of their opposite configuration, only their α-pyridone moieties overlap well and maintain similar principal interactions.

as a starting model for refinement, initially by rigid body refinement (20−4 Å resolution), followed by simulated annealing (SA) and individual *B*-factor (IB) refinements [20−2.1 Å resolution for (+)-HupA and 20−2.35 Å resolution for (−)-HupB] using CNS. Maps were calculated using all of the data ($F > 0\sigma$). Chemical models of the inhibitors were modeled into the largest positive peaks of the $F_o - F_c$ difference maps, which in both cases were seen near the bottom of the active site gorge. The structure was then refined by positional maximum-likelihood minimization, followed by individual *B*-factor refinement (*45*). Following this, water molecules were added, using the molecular graphics program O (*46*), and the *R*-factors converged (see Table 2). The coordinates of both refined structures and the corresponding structure factors have been deposited in the PDB [ID codes 1GPK for *Tc*AChE/(+)-HupA and 1GPN for *Tc*AChE/(−)-HupB].

RESULTS

Inhibition of TcAChE by Huperzines. Steady-state measurements of *Tc*AChE activity in the presence of (−)-HupB, (+)-HupA, and (−)-HupA reveal that V_{maxi} values (values of V_{max} at a given inhibitor concentration) decrease as a function of inhibitor concentration, while the corresponding K_{app} values (observed K_m values at that inhibitor concentration) increase (Figure 2). In addition, the right-hand side of Figure 2 shows that the dependence of K_{app}/V_{maxi} values on the concentration of all three compounds is linear. Linear mixed-type inhibition is typified by these two features. K_i values obtained from the slopes of the linear fitted lines in Figure 2 are given in Table 3. The most powerful inhibitor of the three is (−)-HupA, which is ca. 25-fold and 2-fold stronger than (+)-HupA and (−)-HupB, respectively.

It was already shown that (−)-HupA binds more tightly to mammalian AChE than to *Tc*AChE (*33*). This difference, which ranges from 5- to 40-fold depending on the source of enzyme, was ascribed to the presence of a tyrosine residue in mammalian AChE at the position equivalent to Phe330 in *Tc*AChE (*35*). Nevertheless, our data show that the order of binding affinities, (−)-HupA > (−)-HupB ≫ (+)-HupA, for mammalian AChE is maintained for *Tc*AChE.

Refinement and Map Fitting. X-ray data for the trigonal crystals (see Table 1) of *Tc*AChE soaked with both (−)-HupB and (+)-HupA were collected and refined to 2.35 and 2.1 Å resolution, respectively (Table 2). The locations of the binding sites for (−)-HupB and (+)-HupA in the active site of *Tc*AChE were readily detected in the initial $F_o - F_c$ maps (calculated after the first cycle of refinement) as 6.7 and 5.0 σ peaks, respectively. Only the (−) configuration of HupB (natural isomer) and the (+) configuration of HupA (unnatural isomer) could be modeled into these peaks. The refinements permitted assignment of 289 and 529 water molecules, respectively, to the structures of *Tc*AChE/(−)-HupB and *Tc*AChE/(+)-HupA. The *R*-factors decreased continuously during refinement of both structures and finally converged to the values given in Table 2.

Ligand Binding Sites. As expected from the high degree of chemical similarity between HupA and HupB (Figure 1), the binding site for (−)-HupB in *Tc*AChE is very similar to

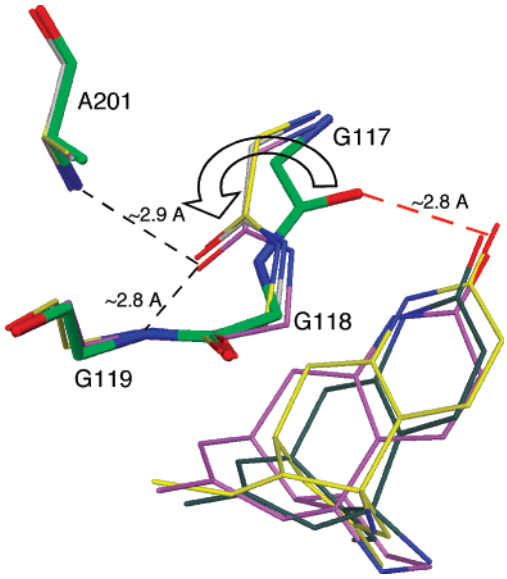

FIGURE 6: Flip of the peptide bond between Gly117 and Gly118 in the active site of *Tc*AChE upon binding of huperzine inhibitors. Four structures of *Tc*AChE are superimposed: native (green; PDB code 2ACE) and three structures in complex with (−)-HupB (purple), (+)-HupA (yellow), and (−)-HupA (gray). All ligands share a carbonyl oxygen atom at a similar position, which appears to repel the main chain carbonyl oxygen of Gly117. This presumed carbonyl−carbonyl repulsion is shown as a red dashed line of average distance of 2.8 Å. The flipped carbonyl of Gly117 is then stabilized through H-bond interactions with the NH groups of Gly119 and Ala201, both of which are part of the oxyanion hole.

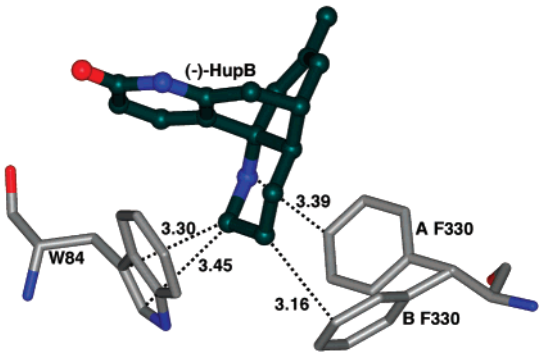

FIGURE 7: Interaction of (−)-HupB with the anionic site of *Tc*AChE. (−)-HupB is shown as a ball-and-stick model (dark green) and amino acid residues as stick models (gray); oxygen and nitrogen are colored red and blue, respectively. All distances from the D ring of (−)-HupB (Figure 1) to either Phe330 or Trp84, which are shorter than 3.5 Å, are shown. On the basis of the observed distances the interactions can be characterized either as van der Waals or as X−H···π H-bonds (X here stands for carbon or nitrogen). Phe330 was refined in two alternative conformations: the A conformation, which is similar to that seen for complexes with both (+)- and (−)-HupA, was refined with 65% occupancy, and the B conformation with only 35% occupancy.

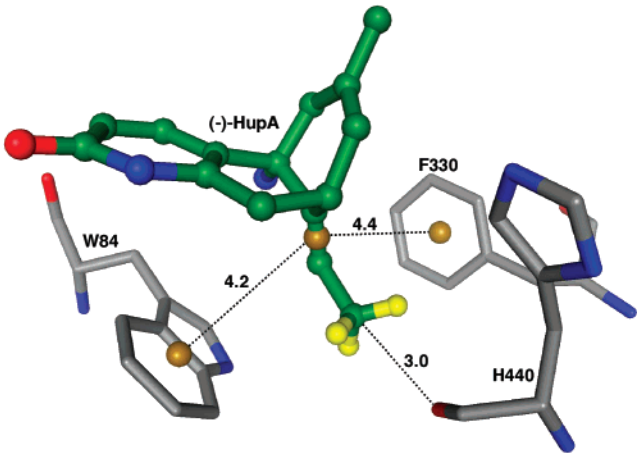

FIGURE 8: Interaction of (−)-HupA with the anionic site of *Tc*AChE. (−)-HupA is shown as a ball-and-stick model (green), protein residues are shown as sticks (gray), and centroids are shown as brown balls; oxygen, nitrogen, and hydrogen atoms are colored red, blue, and yellow, respectively. In addition to the H-bond, already noted, between the ethylidene methyl group of (−)-HupA and the main chain oxygen of His440 (16), the figure shows a putative interaction between the C10−C11 double bond of (−)-HupA and the aromatic ring systems of Phe330 and Trp84.

that seen in the *Tc*AChE/(−)-HupA complex (PDB code 1VOT). All of the protein residues in the vicinity of the bound (−)-HupB, except for Phe330, are in conformations very similar to those seen in the *Tc*AChE/(−)-HupA structure (Figure 3). Phe330 was refined in two alternative conformations in the *Tc*AChE/(−)-HupB structure, one (65% occupancy) very similar to that seen in the *Tc*AChE/(−)-HupA structure and another distinct conformation (35% occupancy). This is the first reported case of discrete disorder for Phe330 in a particular AChE structure. Figure 3 also shows that the water network around (−)-HupB is similar to that seen around (−)-HupA, which was suggested to stabilize its complex with *Tc*AChE (*16*).

The binding site for (+)-HupA in *Tc*AChE is also part of that for (−)-HupA. However, unlike its α-pyridone moiety (ring A in Figure 1) which overlaps well with that of

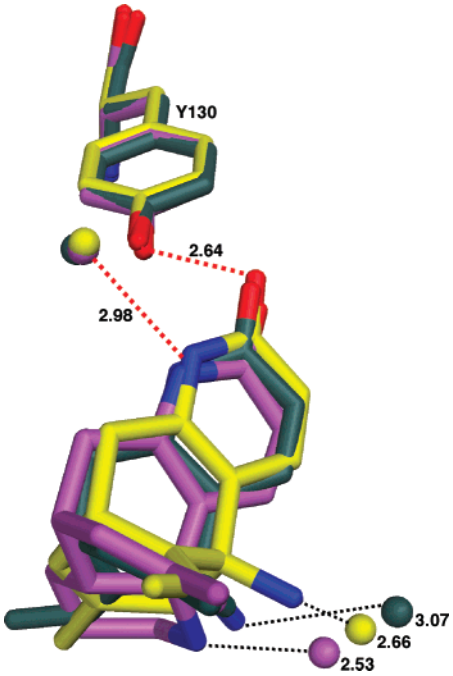

FIGURE 9: Hydrogen bond interactions shared by (−)- and (+)-HupA and (−)-HupB. Superposition of the structures of *Tc*AChE complexed with (−)-HupA (gray), (+)-HupA (yellow), and (−)-HupB (orchid) show that the α-pyridone moiety, which is common to all three of the ligands, is the best overlapping unit. This seems to be governed by two conserved H-bonds, indicated as red dashed lines with their average distance in angstroms and a standard deviation of only 0.06 Å. Another conserved H-bond is made by the amino group of both (−)- and (+)-HupA and by the ring C nitrogen of (−)-HupB, to a water molecule, shown as black dashed lines. In this case the water molecules in question are not in direct interaction with the protein, and their positions are less conserved; thus, the variation in distances is rather high.

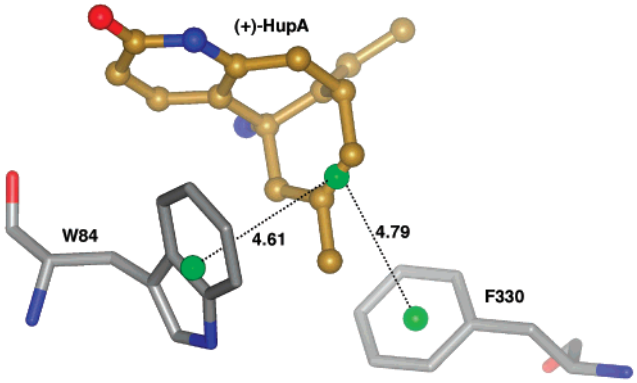

FIGURE 10: Interactions of (+)-HupA with the anionic site of *Tc*AChE. (+)-HupA is displayed as a ball-and-stick model (brown), amino acid residues are depicted as sticks (gray), and centroids for the aromatic rings and of the double bond of (+)-HupA are shown as green balls; oxygen and nitrogen atoms are colored red and blue, respectively. The interactions seen (distances in angstroms) may partially mimic the $\pi-\pi$ interactions seen for the enantiomorph inhibitor (Figure 8). No X−H···π H-bonds of length <3.7 Å are observed between the three-carbon bridge of (+)-HupA and the anionic site.

(−)-HupA, the ethylidene methyl group of (+)-HupA points in the opposite direction to that of (−)-HupA, occupying similar space to that occupied by the three-carbon bridge of (−)-HupA in its *Tc*AChE complex (Figure 4). The cyclic carbon, to which the primary amine of (+)-HupA is attached, overlaps well with the corresponding carbon of (−)-HupA.

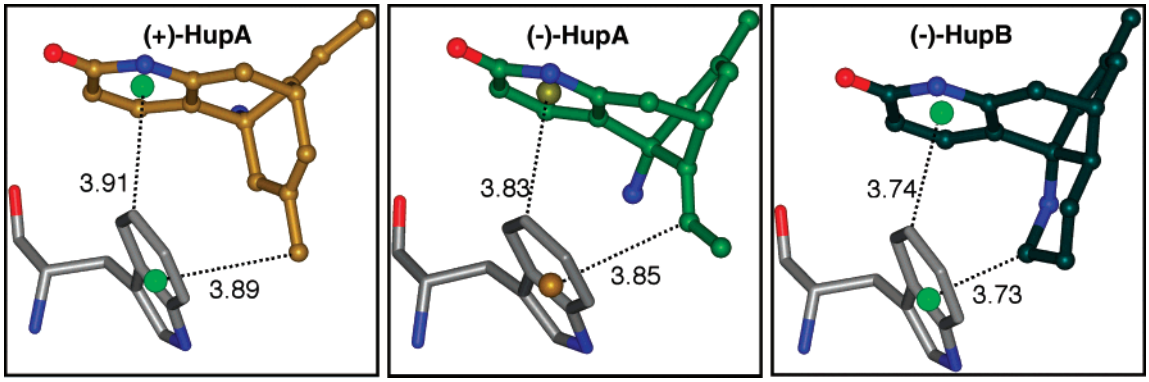

FIGURE 11: Possible mutual C−H···π interactions utilized by HupA and its analogues for binding to *Tc*AChE. Each of the above inhibitors has an aromatic ring (α-pyridone) which may serve as a hydrogen acceptor and other group which serves as a hydrogen donor. The aromatic residue at position 84 within the anionic site of *Tc*AChE can also serve as both hydrogen acceptor and donor. The position and orientation of these inhibitors in the active site allow them to interact with Trp84 as both hydrogen donors and acceptors. Distances from centroids of the aromatic rings (shown as balls) to carbons of the corresponding C−H groups are given in angstroms.

However, due to opposite handedness, their primary amines, which are most likely protonated at physiological pH, diverge (Figure 4), giving rise to different arrangements for the water networks with which they are in contact (Figure 5). The amino acid residues of the binding sites for these two ligands are in very similar conformations (Figure 5).

Like (−)-HupA, both (+)-HupA and (−)-HupB cause a peptide bond flip (*46*) between Gly117 and Gly118 (Figure 6). This seems to be induced by the carbonyl oxygen common to all three ligands. In all three complexes, this carbonyl oxygen forms a short hydrogen bond (H-bond) interaction with the hydroxyl of Tyr130 (see below). The partial negative charge of the carbonyl oxygen so positioned appears to repel the carbonyl oxygen of Gly117 and thus is the underlying cause of the peptide bond flip. The flipped carbonyl of Gly117 is then stabilized by ∼2.9 and ∼2.8 Å H-bonds, respectively, with Gly119 NH and Ala201 NH in all three complexes (Figure 6).

DISCUSSION

Structural Comparison of TcAChE/(−)-HupB and TcAChE/(−)-HupA. Comparison of the structures of the two complexes shows that the only significant differences involve the interaction of ring C of (−)-HupB and of the ethylidene of (−)-HupA with the enzyme. In contrast to the prediction made on the basis of the structure of the *Tc*AChE/(−)-HupA complex (*16*), the additional ring in (−)-HupB (ring C) does not clash with Trp84. Instead, it fits the binding site very well, interacting with Trp84 and Phe330 (Figure 7). The aromatic properties of this site allow it to serve as a π-type hydrogen acceptor, with which X−H groups may form nonconventional H-bonds (*47*, *48*). However, the distances shown in Figure 7 are also consistent with van der Waals interactions. Thus, the interactions of ring C of (−)-HupB with the anionic site involve either van der Waals interactions or weak H-bonds of type C−H···π. Indeed, we see that C9 and C10 in ring C of (−)-HupB may form such bonds with Trp84 and Phe330, respectively, in addition to the interaction of the nitrogen of ring C with the latter.

(−)-HupA, which lacks ring C of (−)-HupB, utilizes the distal carbon, C10, of its ethylidene group to make a C−H···O H-bond with H440O (Figure 8). The π electrons of the double bond between C11 and C12 of this group may interact with Phe330 and Trp84 through $\pi-\pi$ stacking. A similar interaction appears to occur between the cyclohexene double bond of galanthamine and Trp84 (*15*). Although (−)-HupB appears to make more interactions with the anionic site than (−)-HupA (compare Figures 7 and 8), it seems plausible that the additional interaction of (−)-HupA C10 with His440O dominates these interactions and thus is responsible for its 2-fold higher affinity.

Structural Comparison of TcAChE/(+)-HupA and TcAChE/(−)-HupA. The stereochemical similarity between huprine X and the (+) configuration of HupA led us to suggest that the latter may orient itself similarly to huprine X within the active site of *Tc*AChE (*35*). In such an orientation, its α-pyridone group (ring A) would point in the opposite direction to that of (−)-HupA in its corresponding *Tc*AChE complex. That suggestion was implicitly based on the assumption that the mode of interaction of HupA with *Tc*AChE is governed primarily by its carbobicyclic moiety, which is also present in huprine X. However, the crystal structure of the *Tc*AChE/(+)-HupA complex reveals that the α-pyridone moieties of (+)- and (−)-HupA are oriented very similarly in their respective complexes (Figures 4 and 5). The key interactions made by the α-pyridone ring of (−)-HupA are thus maintained in the *Tc*AChE/(+)-HupA complex (Figure 9). To accomplish this, (+)-HupA must be flipped over relative to (−)-HupA, so that its ethylidene methyl group points away from the "anionic" site while its three-carbon bridge occupies the space facing it (Figures 4 and 5).

The immediate conclusion from the above observation is that the most powerful interaction made by HupA and its analogues can be attributed to their α-pyridone moiety, which makes two short H-bonds, one with Tyr130 and one with a conserved water molecule. These interactions are shared by (−)-HupB, (+)-HupA, and (−)-HupA and have average lengths of 2.64 ± 0.06 and 2.98 ± 0.06 Å, respectively (Figure 9). A more tentative conclusion can be made about the similarity between the three-carbon bridge and the ethylidene methyl group of HupA. Although (+)-HupA is less active than the natural (−) configuration, the fact that it still inhibits *Tc*AChE significantly (Table 3) suggests that the interaction made by the ethylidene methyl group of (−)-HupA with the anionic site may be replaced by a similar interaction by the bridging moiety of (+)-HupA. Figure 10 shows that the double bond between C8 and C15 in the three-

carbon bridge of (+)-HupA may mimic the $\pi-\pi$ interactions made by the ethylidene group of (−)-HupA (Figure 8). The ca. 25-fold difference in activity measured between the two enantiomorphs may be partially ascribed to the fact that the H-bond between the ethylidene methyl of (−)-HupA and His440O is absent in the (+)-HupA complex. As mentioned above, this interaction is also absent in the *Tc*AChE/(−)-HupB complex but seems to be compensated for by the presence of more C−H$\cdots\pi$/van der Waals interactions shown in Figure 7.

Interaction Motifs Employed by the Huperzine Family. As already pointed out, the α-pyridone moiety common to all three inhibitors appears to be the most dominant pharmacophore, interacting via two conserved H-bonds (Figure 9). The question which arises is whether these interactions, in conjunction with the interactions seen with the anionic site, and with His440 in the case of (−)-HupA, can adequately explain the affinities of these inhibitors and their shared capacity to disrupt the oxyanion hole (see below). To address this point, we have carefully examined the structures of all three complexes in a search for interactions not reported for the (−)-HupA complex (*16*) and shared by all three ligands. We have thus been able to identify novel interactions that may contribute to the short-range fixation of the orientation shared by the three ligands. These may include mutual C−H$\cdots\pi$ interactions (*47*), in which the aromatic π electrons of the indole ring of Trp84 serve as the hydrogen acceptor for a nonaromatic C−H group in the ligand, while the indole ring also serves as a hydrogen donor for the aromatic π electrons of the α-pyridone moiety of the inhibitor (Figure 11). Although the distances shown are relatively long, the mutual C−H$\cdots\pi$ interaction motif may play a significant role in the short-range orientation of the inhibitors, since a single residue interacts with two distal units of the inhibitor. It should be noted that the mutual C−H$\cdots\pi$ interactions described above might only be a discrete part of a continuum of van der Waals contacts, all of which contribute to the interaction energies of the ligands with the anionic site.

Disruption of the Oxyanion Hole. The most striking observation seen in the structures of all three huperzine complexes is the flip of the peptide bond between Gly117 and Gly118. This flipped conformation appears to be induced by a carbonyl−carbonyl repulsion (Figure 6). The new conformation is stabilized by Gly117O making H-bonds with Gly119N and Ala201N, the other two functional elements of the three-pronged oxyanion hole characteristic of AChE (*49*). As a consequence, the position of the main chain nitrogen of Gly118 in the oxyanion hole is occupied by the carbonyl of Gly117. It has been conjectured that the peptide flip itself is responsible for the low on-rates observed for inhibition of AChE by (−)-HupA (*16*, *35*). Similarly, its stabilization may contribute to the low rates of dissociation observed (*36*).

The role of the oxyanion hole in the hydrolysis of ACh was clearly evident from the structure of the complex with *Tc*AChE of the transition state analogue, TMTFA, which also binds to the anionic site (*50*). However, unlike cationic substrates, some neutral substrates, such as phenyl acetate and indophenyl acetate, are hydrolyzed by AChE even when the anionic site is modified (*51*, *52*). Thus, hydrolysis of such substrates may still occur in the presence of inhibitors which block the anionic subsite but do not affect the catalytic subsite (catalytic triad, acyl pocket, and the oxyanion hole). The huperzine molecules affect both subsites. They thus would be expected to prevent hydrolysis of all ester substrates, whether charged or neutral.

REFERENCES

1. Marchbanks, R. M. (1982) *J. Neurochem. 39*, 9−15.
2. Katzman, R. (1986) *N. Engl. J. Med. 314*, 964−973.
3. Coyle, J. T., Price, D. L., and DeLong, M. R. (1983) *Science 219*, 1184−1190.
4. Rosenberry, T. L. (1975) *Adv. Enzymol. 43*, 103−218.
5. Dunnett, S. B., and Fibiger, H. C. (1993) *Prog. Brain Res. 98*, 413−420.
6. Weinstock, M. (1997) *J. Neural Transm., Suppl. 49*, 93−102.
7. Bartus, R. T., Dean, R. L., Beer, B., and Lippa, A. S. (1982) *Science 217*, 408−414.
8. Davis, K. L., and Powchik, P. (1995) *Lancet 345*, 625−630.
9. Kawakami, Y., Inoue, A., Kawai, T., Wakita, M., Sugimoto, H., and Hopfinger, A. J. (1996) *Bioorg. Med. Chem. 4*, 1429−1446.
10. Enz, A., Boddeke, H., Gray, J., and Spiegel, R. (1991) *Ann. N.Y. Acad. Sci. 640*, 272−275.
11. Harvey, A. L. (1995) *Pharmacol. Ther. 68*, 113−128.
12. Zhang, R. W., Tang, X. C., Han, Y. Y., Sang, G. W., Zhang, Y. D., Ma, Y. X., Zhang, C. L., and Yang, R. M. (1991) *Acta Pharmacol. Sin. 12*, 250−252.
13. Harel, M., Schalk, I., Ehret-Sabatier, L., Bouet, F., Goeldner, M., Hirth, C., Axelsen, P., Silman, I., and Sussman, J. L. (1993) *Proc. Natl. Acad. Sci. U.S.A. 90*, 9031−9035.
14. Kryger, G., Silman, I., and Sussman, J. L. (1999) *Structure 7*, 297−307.
15. Greenblatt, H. M., Kryger, G., Lewis, T., Silman, I., and Sussman, J. L. (1999) *FEBS Lett. 463*, 321−326.
16. Raves, M. L., Harel, M., Pang, Y. P., Silman, I., Kozikowski, A. P., and Sussman, J. L. (1997) *Nat. Struct. Biol. 4*, 57−63.
17. Bar-On, P., Millard, C. B., Harel, M., Dvir, H., Enz, A., Sussman, J. L., and Silman, I. (2002) *Biochemistry 41*, 3555−3564.
18. Liu, J. S., and Zhu, Y. L. (1986) *Can. J. Chem. 64*, 837−839.
19. Bai, D. L., Tang, X. C., and He, X. C. (2000) *Curr. Med. Chem. 7*, 355−374.
20. Wang, Y. E., Yue, D. X., and Tang, X. C. (1986) *Acta Pharmacol. Sin. 7*, 110−113.
21. Kozikowski, A. P., Xia, Y., Reddy, E. R., Tuckmantel, W., Hanin, I., and Tang, X. C. (1991) *J. Org. Chem. 56*, 4636−4645.
22. Liu, J. S., Zhang, H. Y., Wang, L. M., and Tang, X. C. (1999) *Acta Pharmacol. Sin. 20*, 141−145.
23. Badia, A., Baños, J. E., Camps, P., Contreras, J., Görbig, D. M., Muñoz-Torrero, D., Simón, M., and Vivas, N. M. (1998) *Bioorg. Med. Chem. 6*, 427−440.
24. Carlier, P. R., Du, D. M., Han, Y., Liu, J., and Pang, Y. P. (1999) *Bioorg. Med. Chem. Lett. 9*, 2335−2338.
25. Carlier, P. R., Du, D. M., Han, Y. F., Liu, J., Perola, E., Williams, I. D., and Pang, Y. P. (2000) *Angew. Chem., Int. Ed. Engl. 39*, 1775−1777.
26. Zhu, X. D., and Tang, X. C. (1988) *Acta Pharmacol. Sin. 9*, 492−497.
27. Zhu, X. D., and Tang, X. C. (1987) *Acta Pharm. Sin. 22*, 812−817.
28. Tang, X. C., Zhu, D. Y., and Lu, W. H. (1988) in *Current Research in Alzheimer Therapy: Cholinesterase Inhibitors* (Giacobini, E., and Becker, R., Eds.) pp 289−294, Taylor and Francis, New York.
29. Wang, X. D., Zhang, J. M., Yang, H. H., and Hu, G. Y. (1999) *Acta Pharmacol. Sin. 20*, 31−35.
30. Wang, H. B., Wang, X. C., Zhang, S. Q., and Lou, C. H. (1999) *Acta Bot. Sin. 41*, 364−368.
31. Zhang, Y. H., Chen, X. Q., Yang, H. H., Jin, G. Y., Bai, D. L., and Hu, G. Y. (2000) *Neurosci. Lett. 295*, 116−118.
32. Zhang, H. Y., Liang, Y. Q., Tang, X. C., He, X. C., and Bai, D. L. (2002) *Neurosci. Lett. 317*, 143−146.
33. Saxena, A., Qian, N., Kovach, I. M., Kozikowski, A. P., Pang, Y. P., Vellom, D. C., Radic, Z., Quinn, D., Taylor, P., and Doctor, B. P. (1994) *Protein Sci. 3*, 1770−1778.
34. McKinney, M., Miller, J. H., Yamada, F., Tuckmantel, W., and Kozikowski, A. P. (1991) *Eur. J. Pharmacol. 203*, 303−305.
35. Dvir, H., Wong, D. M., Harel, M., Barril, X., Orozco, M., Luque, F. J., Munoz-Torrero, D., Camps, P., Rosenberry, T. L., Silman, I., and Sussman, J. L. (2002) *Biochemistry 41*, 2970−2981.
36. Ashani, Y., Peggins, J. O., and Doctor, B. P. (1992) *Biochem. Biophys. Res. Commun. 184*, 719−726.

37. He, X. C., Wang, B., Yu, G., and Bai, D. (2002) *Tetrahedron: Asymmetry* (in press).
38. Sussman, J. L., Harel, M., Frolow, F., Varon, L., Toker, L., Futerman, A. H., and Silman, I. (1988) *J. Mol. Biol. 203*, 821−823.
39. Ellman, G. L., Courtney, K. D., Andres, V., Jr., and Featherstone, R. M. (1961) *Biochem. Pharmacol. 7*, 88−95.
40. Hope, H., Frolow, F., and Sussman, J. L. (1987) *Rigaku J. 4*, 3−10.
41. Hope, H. (1988) *Acta Crystallogr. B44*, 22−26.
42. Ravelli, R. B. G., Sweet, R. M., Skinner, J. M., Duisenberg, A. J. M., and Kroon, J. (1997) *J. Appl. Crystallogr. 30*, 551−554.
43. Otwinowski, Z., and Minor, W. (1997) *Methods Enzymol. 276*, 307−326.
44. Bailey, S. (1994) *Acta Crystallogr. D50*, 760−763.
45. Brünger, A. T., Adams, P. D., Clore, G. M., DeLano, W. L., Gros, P., Grosse-Kunstleve, R. W., Jiang, J. S., Kuszewski, J., Nilges, M., Pannu, N. S., Read, R. J., Rice, L. M., Simonson, T., and Warren, G. L. (1998) *Acta Crystallogr. D54*, 905−921.
46. Jones, T. A., Zou, J.-Y., Cowan, S. W., and Kjeldgaard, M. (1991) *Acta Crystallogr. A47*, 110−119.
47. Desiraju, F. R., and Steiner, T. (1999) *The Weak Hydrogen Bond*, Oxford University Press, New York.
48. Braga, D., Grepioni, F., and Tedesco, E. (1998) *Organometallics 17*, 2669−2672.
49. Sussman, J. L., Harel, M., Frolow, F., Oefner, C., Goldman, A., Toker, L., and Silman, I. (1991) *Science 253*, 872−879.
50. Harel, M., Quinn, D. M., Nair, H. K., Silman, I., and Sussman, J. L. (1996) *J. Am. Chem. Soc. 118*, 2340−2346.
51. Fuchs, S., Gurari, D., and Silman, I. (1974) *Arch. Biochem. Biophys. 165*, 90−97.
52. Purdie, J. E., and McIvor, R. A. (1966) *Biochim. Biophys. Acta 128*, 590−593.

BI020151+